Energy 90 (2015) 864–878

Contents lists available at ScienceDirect

Energy

journal homepage: www.elsevier.com/locate/energy

Operation of an organic Rankine cycle dependent on pumping flow rates and expander torques

Xufei Yang, Jinliang Xu*, Zheng Miao, Jinghuang Zou, Chao Yu

The Beijing Key Laboratory of Multiphase Flow and Heat Transfer, North China Electric Power University, 102206 Beijing, China

ARTICLE INFO

Article history:
Received 12 December 2014
Received in revised form
19 June 2015
Accepted 27 July 2015
Available online 20 August 2015

Keywords:
Organic Rankine cycle
Pump
Expander
Thermodynamic
Heat transfer

ABSTRACT

An ORC (organic Rankine cycle) was developed with R123 as the working fluid. The heat capacity is in ~100 kW. The match between pump and expander is investigated. Lower pump frequencies ($f < 10$ Hz) adapt the whole range of expander torques, yielding stable flow. Higher pump frequencies ($f > 10$ Hz) adapt low expander torques only, and cause unstable flow and pump cavitation for larger expander torques. Ultra-low expander torques generate sufficiently high vapor superheatings to decrease expander efficiencies. Ultra-high expander torques achieve saturation vapor at the expander inlet, causing liquid droplets induced shock wave to worsen expander performance. An optimal range of expander torques exists to have better expander performance. A liquid subcooling of 20 °C is necessary to avoid pump cavitation. Expander powers and efficiencies show parabola shapes versus expander torques, or vapor superheatings at the expander inlet. The optimal vapor superheating is 13 °C. The cavitation mechanisms and measures to avoid cavitation are analyzed. This paper notes the overestimation of ORC performance by equilibrium thermodynamic analysis. Assumptions should be dependent on experiments. Future studies are suggested on organic fluid flow, heat transfer and energy conversion in various components.

1. Introduction

The energy shortage and environment pollution encourage us to develop new and clean energy technologies. The low grade thermal energy with the temperature of less than 250 °C has received great attention worldwide [1]. ORC (organic Rankine cycle) is an important system to recover low grade thermal energy [2,3], including geothermal energy [4–7], solar energy [8–11], waste heat in various industry sectors [12–19] and biomass thermal energy [20–22].

Many investigations have been performed for ORCs. The work focused on equilibrium thermodynamic analysis and fluid selection. ORCs can be classified as subcritical pressure ORC, transcritical pressure ORC and ORC with mixture working fluid [23]. Based on heat source temperatures and computation conditions, the recommended organic fluids are quite different [16,24–26]. Generally, due to better thermal match of organic fluid and heat carrier fluid of heat source in the evaporator, transcritical pressure ORC and ORC with mixture fluid have better performance than subcritical pressure ORCs [16,27,28]. For subcritical pressure ORCs, isothermal evaporation heat transfer takes place in the evaporator to increase exergy destruction. However, subcritical pressure ORCs attract industries due to low pressure operation and easy fluid selection.

From thermodynamic cycle point of view, saturation vapor at the expander inlet achieves higher thermal efficiency. Fewer authors investigated ORCs at superheating vapor cases at the expander inlet [19,29,30]. Saturation vapor at the expander inlet may cause following issues: (1) liquid droplets are entrained in vapor to worsen the expander performance; (2) wet expansion happens in the expander, which should be avoided; (3) the fluid state (either two-phase mixture or saturation vapor) cannot be judged by pressure and temperature only.

Besides, thermodynamic analysis has several ideal assumptions which should be further verified by experiments. For instance, isentropic efficiency of expanders was assumed to be 75–87% [25,31,32], which is higher than practical values. Many theoretical studies assume higher pressures in the range of 2.5–32.67 MPa [10,16,29,31], but experimental studies operate ORCs with the pressure of ~1 MPa (see Table 1). The temperature difference at the pinch point, vapor superheating at the expander inlet and liquid subcooling at the pump inlet are assumed to be not changed during operation. All these assumptions should be verified by experiments.

* Corresponding author. Tel./fax: +86 10 61772613.
E-mail address: xjl@ncepu.edu.cn (J. Xu).

http://dx.doi.org/10.1016/j.energy.2015.07.121
0360-5442/

Table 1
The literature survey on ORCs.

Ref.	Heat source & working fluid	Expander & pump types	Major parameters	Comments
[13]	Flue gas, 90–220 °C; R123	Scroll expander; multistage centrifugal pump	P_{eva} = 0.56–1.08 MPa W_{exp} = 0.16–0.65 kW $\eta_{exp,s}$ = N/A η_{th} = 2–8.5%	Both expander shaft power and pump consumption power were computed by the enthalpy difference. The output power was below 1 kW.
[18]	Diesel engine exhaust gas, 417–485 °C; R123	Single screw expander; multistage centrifugal pump	P_{eva} = 1.34 MPa W_{exp} = 10.38 kW $\eta_{exp,s}$ = 73.25% η_{th} = 6.48%	The expander shaft power was determined by dynamometer. The heat source temperature was extremely high. The thermal efficiency was lower than 5%.
[35]	Hot air, 105 °C; R245fa	Scroll expander; metering pump	P_{eva} = 0.5–1.0 MPa W_{exp} = 0.151 kW $\eta_{exp,s}$ = 41–72% η_{th} = 1.7–3.2%	Both expander shaft power and pump consumption power were computed by the enthalpy difference. The output power was below 1 kW, and the thermal efficiency was lower than 5%.
[37]	Hot water, 77.3 °C; R134a	Scroll expander; piston-diaphragm pump	P_{eva} = 22 bar W_{exp} = 2.05 kW $\eta_{exp,s}$ = N/A η_{th} = 4%	The expander shaft power was determined by dynamometer. The evaporating pressure was relatively high. The thermal efficiency was lower than 5%.
[38]	Solar energy, 41–75 °C; R134a	Scroll expander; positive displacement pump	P_{eva} = 3.5–9.5 bar W_{exp} = 0.25–0.92 kW $\eta_{exp,s}$ = N/A η_{th} = 0.73–1.17%	The expander shaft power was determined by dynamometer. The solar energy was unstable, and the actual thermal efficiency was very low.
[39]	Steam, 198 °C; R123	Gerotor expander, scroll expander; gear pump, piston pump	P_{eva} = 1.878–2.041 MPa W_{exp} = 2.07–2.96 kW $\eta_{exp,s}$ = 83–85% η_{th} = N/A	The way to compute the power was not given in the reference. The heat source temperature and evaporating pressure were very high. The piston pump had better performance than gear pump for ORC system.
[40]	Hot air, 101.7–165.2 °C; R123	Scroll expander; diaphragm pump	P_{eva} = 5.45–11.12 bar W_{exp} = 0.382–1.820 kW $\eta_{exp,s}$ = 68% η_{th} = N/A	The way to compute the power was not given. A semi-empirical model of scroll expander was established.
[41]	Conductive oil, 75–130 °C; R245fa, R245fa/R601a (0.72/0.28)	Scroll expander; diaphragm pump	P_{eva} = 3.6–10 bar W_{ele} = 0.2–0.55 kWe $\eta_{exp,s}$ = 71–83% η_{th} = 2.9–4.45%	The expander output power was calculated by the measured voltage and current. Two types of working fluids were compared. The output power was below 1 kW. The thermal efficiency was lower than 5%.
[42]	About 126 °C; HFE 7000	Vane-type expander; pump: N/A	P_{eva} = 6.66–6.724 bar W_{shaf} = 1.69–1.72 kW W_{ele} = 0.8248–0.8607 kWe $\eta_{exp,s}$ = 52.38–55.45% η_{th} = 3.73–3.89% η_{ele} = 1.38–1.40%	Both expander shaft power and pump consumption power were computed by the enthalpy difference. At the same time, the electric power was calculated by the measured voltage and current of the power generation machine. The result showed that the shaft power was overestimated by the enthalpy difference.
[43]	Electric boiler, 120–150 °C; R245fa	Scroll expander; diaphragm pump	P_{eva} = 13–18 bar $W_{exp,ele}$ = 1.5 kWe $\eta_{exp,s}$ = 60–74% η_{th} = 8%	The expander shaft power was calculated by the measured voltage and current of the power generation machine. The thermal efficiency was relatively high.
[44,45]	Pressurized hot water, 115–125 °C; R245fa	Twin screw expander; multistage centrifugal pump	P_{eva} = 1.2–1.4 MPa W_{exp} = 17–50 kW $\eta_{exp,s}$ = N/A η_{th} = 8.05%	The way to compute the power was not given. The output power reached 50 kW, and the thermal efficiency was relatively high.
[46]	Hot water, 85–116 °C; R245fa	Twin screw expander; pump: N/A	P_{eva} = 0.581–0.911 MPa W_{exp} = 15.5–39.9 kW $\eta_{exp,s}$ = N/A η_{th} = 5.6–8.3%	Both expander shaft power and pump consumption power were computed by the enthalpy difference, and the thermal efficiency was relatively high.
[47]	Steam and hot water; R245fa	Radial turbine; centrifugal pump	P_{eva} = 8.65 bar W_{exp} = 32.7 kW $\eta_{exp,s}$ = 78.7% η_{th} = 5.22%	Power output of the turbine was measured by power meter, and the pump consumption power was computed by the enthalpy difference. The thermal efficiency was more than 5%.
[56]	Hot water, 90 °C; R245fa	Scroll expander, trochoidal expander; DC diaphragm pump	P_{eva} = N/A W_{exp} = 7.2–8.4 W W_p = 4.9–5.6 W $\eta_{exp,s}$ = 4.55% η_{th} = 0.16–0.20%	Micro ORC generator was packaged without external power supply. The expander shaft power was determined by torque and speed meter. The thermal efficiency was very low.
[57]	Conductive oil, 140–160 °C; R123	Scroll expander; piston pump	P_{eva} = 0.55–1.5 MPa W_{exp} = 2.35–3.25 kW W_p = 0.2–1 kW $\eta_{exp,s}$ = 45–82% η_{th} = 5.12–6.39%	The expander shaft power was determined by AC dynamometer. The study identified that the measured shaft power was about 15–20% lower than the enthalpy determined value. The result indicated that the shaft power was overestimated by the enthalpy difference. The thermal efficiency was more than 5%.
[58]	Pressurized hot water, 120 °C; R245fa	Scroll expander; plunger pump	P_{eva} = 0.55–1.5 MPa W_{exp} = 1.7–3.4 kW W_p = N/A $\eta_{exp,s}$ = 60.9–61.2% η_{th} = 7.5%	ORC with multiple expanders used in parallel (PE-ORC) for large variation waste heat source. The expander shaft power was determined by torque and speed. The thermal efficiency was relatively high.
[59]	Exhaust gas for capstone diesel turbine, 302.7 °C; R245fa/R365mfc (0.485/0.515)	Scroll expander; plunger pump	P_{eva} = 1.4052 MPa W_{ele} = 0.7 kWe W_p = N/A $\eta_{exp,s}$ = N/A η_{th} = 3.9%	The actual electrical power was measured with the light bulb loading. The pump inlet subcooling temperature of 13 °C was reported. The thermal efficiency was lower than 5%.

(*continued on next page*)

Table 1 (*continued*)

Ref.	Heat source & working fluid	Expander & pump types	Major parameters	Comments
[60]	Exhaust gas of diesel engine, 408 °C; R123	Single screw expander; multistage centrifugal pump	P_{eva} = 1.05 MPa W_{exp} = 5.12 kW W_p = N/A $\eta_{exp,s}$ = 49.5% η_{th} = 7–8%	The expander shaft power was determined by torque and speed. The single screw expander performance was reported. The thermal efficiency was relatively high.
[61]	163–165 °C; R245fa	Commercial ORC module	P_{eva} = 27.2–29.44 bar W_{ele} = 3.89–6.90 kWe W_p = 1.06–1.30 kWe $\eta_{exp,s}$ = 65% η_{th} = 8.80%	Commercial ORC module was used for micro combined heat and power (CHP) applications. The electrical power output and electrical pump consumption were directly measured. The thermal efficiency was relatively high.

The ORC prototypes were developed by various research groups. The power generation was below 50 kW. Most of them were in ~1 kW scale [13,33,34,37–43]. Few studies reported power output in 10 kW scale [45–47] (see Table 1). There are three methods to compute the expander power: (1) The power was computed by mass flow rate and enthalpy difference between expander inlet and outlet ($W_{exp,cal}$) [33]; (2) The power was determined by shaft torque and rotating speed of the expander (W_{exp}) [37]; and (3) The power was calculated by measured voltage and current of the power generation machine (W_{ele}) [42]. Among the three methods, the power measured by the torque and rotating speed of the expander approaches the real value, well reflecting the expander operation.

Most of small scale volume-type expanders are modified from commercial compressors [48]. The small scale velocity-type expanders are designed and fabricated in Refs. [32,47]. The expander suitable for ORCs is in the infancy stage. The pump is an important component, but it has received less attention. The measured pump efficiency was only 7–25% [49], which is smaller than the assumed value of 65–85% in Ref. [50]. The commonly used organic fluids evaporate easily to cause cavitation to weaken pump performance. The system operation strongly depends on the match among various components of the system, which are commented as follows.

The match between heat source and ORC: The ORC performance is strongly affected by heat source. If the heat source temperatures and/or flow rates of the heat carrier fluid are increased, the pressure and temperature are increased to raise power output. The pumping flow rate should be raised to adapt this change. The fluid overpressure may happen to break up ORC. On the other hand, the decreased heat received from the heat source decreases power output and system efficiency to worsen the economic behavior.

The match between pump and expander: The term "match" refers to have good combination parameters between pump and expander to operate ORC effectively and safely. The parameters are capacities, efficiencies, state parameters (pressures, temperatures and enthalpies), etc. The thermodynamic analysis deals with steady ORC operation. The match between pump and expander is useful for both steady and unsteady ORC operation. Ref. [50] proposed the factor of the pumping power related to the expander output, W_p/W_{exp}. One does not know the transient pump and expander parameters on ORC performance. Cayer et al. [51] analyzed CO_2 cycle using a low temperature source.

The match between evaporator and condenser: Evaporation and condensation heat transfer take place in the two heat exchangers. The phase change heat transfer coefficients of organic fluids are significantly lower than those of water. Besides, the phase change heat transfer creates considerable pressure drops, which are neglected in the thermodynamic analysis. Thus, the careful design of heat exchangers is necessary. Two-phase flow and heat transfer should be matched between evaporator and condenser.

Miao et al. [57] described the ORC loop. A scroll expander is connected with an AC dynamometer unit to record shaft power and rotating speed. The ORC can be controlled by two independent parameters: R123 mass flow rate and external load. The maximum measured shaft powers are 2.35 kW at 140 °C and 3.25 kW at 160 °C. The highest thermal efficiencies are 6.39% and 5.12%, at the two temperatures. Miao et al. [57] found that the enthalpy determined power and thermal efficiencies are overestimated compared with measured values.

The thermodynamic analysis sets nearly saturation liquid at pump inlet. Saturation vapor was assumed at expander inlet to yield a higher expander power [17,26]. However, nearly saturation liquid causes pump cavitation. Besides, liquid droplets may be entrained in saturation vapor [45,54], even for dry fluid expansion. When saturation vapor enters expander, droplets attack the expander blade to weaken expander performance. The suitable liquid subcooling at pump inlet and vapor superheating at expander inlet are important for ORC, not only from the thermal efficiency point of view, but also from the safety operation point of view.

The objective of this paper is to investigate match parameters of pump and expander on ORC performance. In order to do so, the ranges of pump frequencies and expander torques are extended to have a set of fluid state parameters at pump and expander inlets. The new finding is that saturation liquid at pump inlet and saturation vapor at expander inlet, specified by equilibrium thermodynamic analysis, are not suitable for practical ORC design and operation. Because ORC works as a liquid–vapor two-phase flow and heat transfer principle, thermal non-equilibrium between two-phases should be considered. This explains why a liquid subcooling of 20.7 °C at pump inlet and a vapor superheating of 13 °C at expander inlet are necessary for present ORC. The equilibrium thermodynamic analysis notes a thermal efficiency penalty when one increases the liquid subcooling at pump inlet and vapor superheating at expander inlet. However, the present paper found that a saturation liquid at pump inlet and saturation vapor at expander inlet cause severe problems such as flow rate decrease and oscillation, noise and vibration. This paper provides the guideline for future ORC design and operation.

2. The ORC experimental setup

2.1. The ORC system design

Fig. 1a shows the developed ORC. The cycle consists of four subsystems, represented by four different colors. The four subsystems are coupled with each other. These subsystems are described as follows.

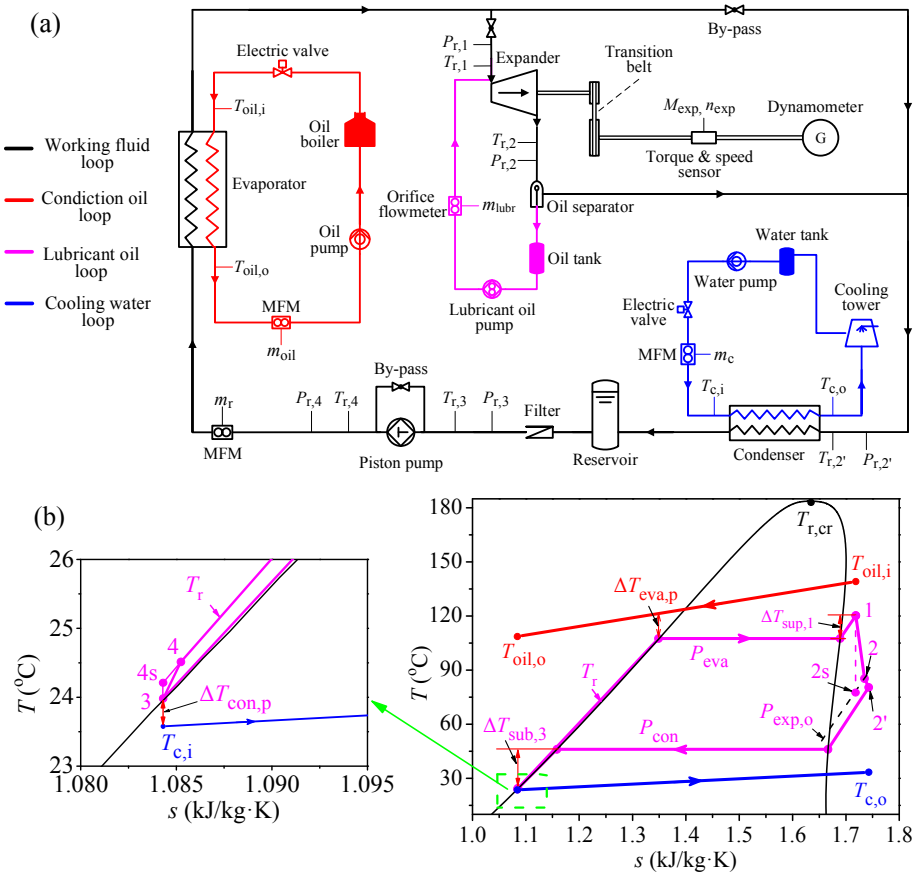

Fig. 1. Developed ORC system and its *T*–*s* cycle.

The organic fluid loop (black color): The ORC loop consists of a piston pump, an evaporator, an expander and a condenser. The piston pump circulates the R123 fluid. It is noted that R123 has been widely used in ORCs [13,18,39,40]. The ORC with R123 fluid has higher thermal efficiencies at heat source temperature below 200 °C [13,29]. The fluid is safety and available from the commercial market. The pump is controlled by a frequency converter to regulate R123 flow rate. The evaporator is a tube-in-tube heat exchanger, having a heat transfer area of 5.53 m^2. The expander is modified from a scroll compressor, which is a commercial product used in air-conditioning system installed in bus. It is considered as one of the promising candidates for the expander in ~kW scale [12,48]. Some modifications are performed so that it is suitable to work as an expander: (1) change the compressor inlet and outlet plenums to yield flow direction of the expander inverse to those of the compressor; (2) change the adapting tube size and valves that are suitable for the expander use; (3) change the seal material and lubrication oil that are suitable for the expander use.

The designed shaft power of the expander is about 4 kW. The condenser is a plate heat exchanger with a heat transfer area of 6.08 m^2. Various instruments are arranged around the ORC loop. The R123 mass flow rate (m_r) is measured by a MFM (mass flow meter). Several measurement points are set around the ORC loop. For instance, points 1, 2, 2′, 3 and 4 refer to expander inlet, expander outlet, condenser inlet, pump inlet and pump outlet. Correspondingly, pressures and temperatures are marked as $P_{r,1}$, $T_{r,1}$, $P_{r,2}$, $T_{r,2}$, $P_{r,2'}$, $T_{r,2'}$, $P_{r,3}$, $T_{r,3}$, $P_{r,4}$, $T_{r,4}$, respectively.

An AC dynamometer dynamically measures the rotating speed (n_{exp}), shaft torque (M_{exp}) and power (W_{exp}) of the expander. The unit consists of a frequency converter, an AC motor, a rotating speed sensor, a monitor, a software and transmission facilities. The power is transmitted by a belt and couplings to the AC motor. The rated rotating speed and maximum shaft torque of the AC motor are 1495 rpm and 70.0 Nm, respectively. The expander rotating speed is two times of that of the AC motor. The computer software dynamically processes the rotating speed and shaft torque of the expander with sensors. The software communicates with the frequency converter to control the shaft torque of the AC motor. During the system operation, the software sets the shaft torque of the AC motor at a specific percentage of the maximum value (70.0 Nm here). The frequency converter of the AC motor controls the shaft torque to maintain the desired value. In such a way, the shaft power of the expander is directly measured. The real pumping power is measured by a pump frequency converter. The measured net power and thermal efficiency are

$$W_{exp} = \frac{2\pi}{60} M_{exp} n_{exp} \tag{1}$$

$$W_{net} = W_{exp} - W_p \tag{2}$$

$$\eta_{th} = \frac{W_{net}}{Q_r} \tag{3}$$

$$\eta_{exp} = \frac{W_{exp}}{m_r(h_1 - h_{2s'})} \tag{4}$$

$$\eta_p = \frac{m_r(h_{4s} - h_3)}{W_p} \tag{5}$$

where W_{exp} and W_p are the measured expander power and pumping power, respectively, Q_r is the total heat received from the

conductive oil, η_{th} is the net ORC thermal efficiency, η_{exp} and η_p are the measured expander efficiency and pump efficiency, respectively. The denominator of Eq. (4) is the isentropic work of the expander. The numerator of Eq. (5) is the isentropic work of the pump.

The conductive oil circuit (red color): The conductive oil is the heat source, heated by an electric heater with a 100 kW capacity. The electric heater automatically adjusts the heating power to satisfy the required oil temperature, which can be up to 300 °C, maximally. The present study uses the oil temperatures of 140 °C, 150 °C and 160 °C to evaporate the R123 fluid. The temperature can be controlled with an uncertainty of 1 °C. An oil pump circulates the conductive oil which receives heat from the electric heater and dissipates heat to the ORC evaporator. The oil mass flow rate (m_{oil}) is measured by MFM. The oil temperature entering and leaving the ORC evaporator are marked as $T_{oil,i}$ and $T_{oil,o}$. The total heat provided by the oil is

$$Q_r = m_{oil} C_P (T_{oil,i} - T_{oil,o}) \tag{6}$$

The Lubricant oil loop (pink color): The expander operation needs lubricant. A gear pump circulates the lubricant. The lubricant is mixed with the R123 vapor at the expander inlet. After the expansion, the lubricant is separated from the R123 vapor by an efficient vapor-oil separator. Then, the lubricant returns to the oil tank.

The cooling water loop (blue color): The cooling water loop is thermally coupled with the ORC condenser. It dissipates extra heat of the ORC system to air environment. The outdoor spray cooling tower is the key component of the cooling water loop. The tower has the cooling capacity of about 73 kW, corresponding to the water flow rate of 5000 kg/h, at which the temperature difference of the cooling water loop is 12.5 °C. Mass flow rate and temperatures are measured to monitor the cooling water loop operation.

2.2. The ORC cycle

Fig. 1b shows the ORC cycle for a practical case. The black envelop is the *T-s* curve of R123, in which $T_{r,cr}$ is the R123 critical temperature. The system is operating at the subcritical pressure. Along the ORC loop, the superheating vapor enters the expander at point 1. The vapor superheating is defined as vapor temperature subtracting saturation temperature: $\Delta T_{sup,1} = T_{r,1} - T_{sat}(P_{r,1})$. The real expansion in the expander is from 1 to 2, indicating an entropy-increase process. Meanwhile, the ideal isentropic process is marked as 1–2s. The isentropic efficiency of the expander is

$$\eta_{exp,s} = \frac{h_1 - h_2}{h_1 - h_{2s'}} \tag{7}$$

where h_1 is the enthalpy determined by pressure and temperature at point 1, h_2 and h_{2s} are the enthalpies at point 2 and $2s'$ (isentropic expansion). The point 2 is at the expander outlet, and $2'$ is at the condenser inlet. The thermodynamic analysis treats the point 2 and $2'$ as the same state. The actual flow from point 2 to $2'$ is due to the pressure drop in the pipeline. In the condenser, the R123 vapor undergoes a single-phase vapor convective heat transfer, an isothermal condensation heat transfer and a subcooled liquid convective heat transfer sections to reach point 3. The near point 3 region is complicated and it is enlarged to Fig. 1b left. The liquid subcooling is defined as $\Delta T_{sub,3} = T_{sat}(P_{r,3}) - T_{r,3}$. The pumping process yields the entropy increase from point 3 to 4, while the ideal isentropic pumping process is from point 3–4s. Thus, the isentropic efficiency of the pump is written as

$$\eta_{p,s} = \frac{h_{4s} - h_3}{h_4 - h_3} \tag{8}$$

The process from point 4 to 1 takes place in the evaporator. The pump mechanical efficiency is defined as the calculated pump work in terms of the enthalpy difference divided by the pump consuming work.

$$\eta_{p,m} = \frac{W_{p,cal}}{W_p} = \frac{\eta_p}{\eta_{p,s}} \tag{9}$$

Eq. (9) states that $\eta_{p,m}$ equals to the measured pump efficiency (η_p) divided by the pump isentropic efficiency ($\eta_{p,m}$). Later we will give $W_{p,cal}$.

Fig. 2a shows the developed ORC, whose components are marked as conduction oil boiler, electric valve, piston pump, condenser, data acquisition system, expander, torque and speed sensor and dynamometer. Fig. 2b shows the enlarged scroll expander and dynamometer. Fig. 2c shows the expander outlook. Fig. 2d–e shows the rotating scroll and fixed scroll of the expander, respectively. Table 2 shows major parameters for piston pump, evaporator, condenser and various heat exchangers. High quality instruments and sensors are used. For instance, pressures, temperatures and mass flow rates are measured by Rosemount 3051 pressure transducer, WRNK 191 temperature sensor and DMF-1-5-A, respectively. The torque and rotating speed are measured by JN-338-100A with the accuracy of 0.1%. The shaft power is measured by the NY 6000 transducer with the accuracy of 1 W. Table 3 shows instruments, sensors and accuracies. The uncertainties of the mass flow rate and enthalpy are 0.2% and 0.6%, respectively.

Different from Refs. [13,35,42,46,47], the shaft torque and power of the expander are measured by instruments, yielding the practical system thermal efficiency. For comparison, the enthalpy decided power of the expander is

$$W_{exp,cal} = m_r (h_1 - h_2) \tag{10}$$

where h_1 and h_2 are determined by pressures and temperatures at the expander inlet and outlet ($P_{r,1}$, $T_{r,1}$, $P_{r,2}$ and $T_{r,2}$), respectively. The enthalpy difference decided pumping power is

$$W_{p,cal} = m_r (h_4 - h_3) \tag{11}$$

The computed thermal efficiency of the ORC system is

$$\eta_{th,cal} = \frac{W_{exp,cal} - W_{p,cal}}{Q_r} \tag{12}$$

It is found that for most cases, the measured thermal efficiency is less than the computed values by Eqs. (10)–(12). Various exergy destructions take place in the expander including heat loss and mechanically induced destructions. The enthalpy drop across the expander is not fully converted to shaft power. Besides, the exergy destruction exists in the piston pump. The pumping power should be larger than that decided by the enthalpy rise across the pump. Therefore, the calculated thermal efficiency is overestimated.

2.3. The operating procedure

The ORC can be operating by specifying mass flow rate, pressure and temperature of the organic fluid. For this ORC prototype, the closed ORC system is initially vacuumed to remove the non-condensable gas. Then, the system is charged by a specific R123 liquid. In such a way, part of the ORC internal volume is occupied by the R123 liquid, and part of the volume is occupied by the R123 vapor. The R123 pressures and temperatures at various locations are not independent parameters, but they are determined by R123 mass flow rate and external load of the expander such as shaft torque and power. The system involves two adjusting parameters:

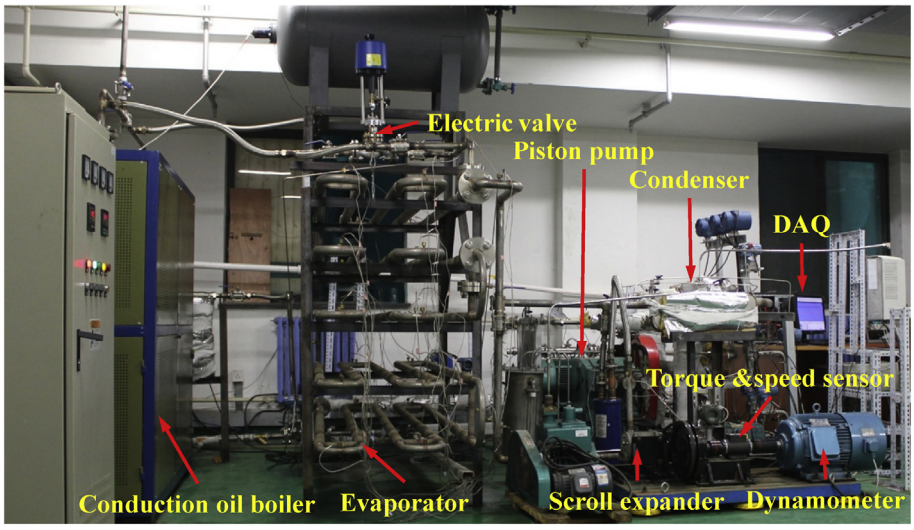

(a)

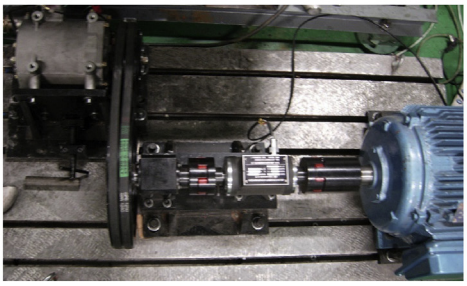

(b)

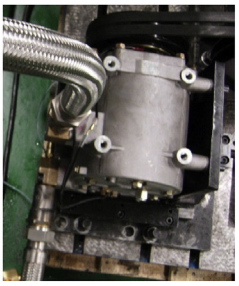

(c)

(d)

(e)

Fig. 2. Photos of developed ORC machine: (a) ORC system; (b) fixed scroll expander and dynamometer; (c) expander; (d) rotating scroll; and (e) fixed scroll.

piston pump frequency and expander torque. Once the two parameters are set, all the state parameters marked in Fig. 1 can be finalized.

Table 4 shows the operating parameters. Three conductive oil temperatures are 140, 150 and 160 °C, respectively. The oil flow rate is 2150 ± 20 kg/h. The cooling water to condense the R123 vapor has the flow rate of 1765 ± 20 kg/h. The piston pump frequencies are in the range of 7–16 Hz. The expander torques are in the range of 2.95–29.7 Nm.

Table 2
Parameters of main components.

Instruments	Parameters
Piston pump	Rated flow rate: 2.5 m^3/h Rated speed: 720 r/min
Evaporator	Heat transfer area: 5.53 m^2
Condenser	Heat transfer area: 6.08 m^2
Heat conducting oil boiler	Heating capacity: 100 kW Temperature control precision: ±1 °C
Cooling tower	Cooling capacity: 73 kW

3. Results and discussion

3.1. Match between pump and expander

Various pumps exist commercially. The most used pumps are multistage pump and reciprocating pump (see Table 1). For

Table 3
Major parameters, instruments and uncertainties.

Parameters	Instruments	Uncertainties
Temperature	WRNK-191	±0.5 °C
Pressure	Rosemount 3051	0.1%
Mass flow rate	DMF-1-5-A	0.2%
Torque & rotation speed	JN-338-100A	0.1%
Shaft power	NY 6000	±1 W

Table 4
Running cases of the experiment.

Parameter	Value
$T_{oil,i}$ (°C)	140, 150, 160
m_{oil} (kg h^{-1})	2150 ± 20
m_c (kg h^{-1})	1765 ± 20
f (Hz)	7, 8, 9, 10, 11, 12, 14, 16
M_{exp} (Nm)	2.95–29.7

multistage pump, flow rate is dependent on rotating speed of pump and pressure at pump outlet. Reciprocating pump includes diaphragm pump and piston pump. For normal operation of reciprocating pump, flow rate is only dependent on rotating speed or piston displacement, but it is not relied on pressure. The piston pump used in this study has the rated flow rate of 2.5 m^3/h and pressure of 6.3 MPa. Because a set of experiments including supercritical pressure ORCs with high pressures will be performed in the future, a high pressure of 6.3 MPa for the pump is selected. The pump pressure does not influence the subcritical pressure ORC experimental results.

Fig. 3a shows the dynamic volume flow rate in a full cycle. The non-dimensional flow rate is defined as $q_r/q_{r,ave}$, where $q_{r,ave}$ is the average volume flow rate. It is found that the minimum and maximum values are 0.907 and 1.047 times of the average value. Fig. 3b shows a linear relationship between volume flow rate and pumping frequency. The maximum flow rate is 2.5 m^3/h at the rotating speed of 720 r/min, corresponding to the 50 Hz frequency.

The ORC external load influences the pump operation. Fig. 4 shows mass flow rates of the pump and expander torque versus time. The conductive oil temperature entering the ORC evaporator is 150 °C and the pump frequency is $f = 9$ Hz. During the long time operation (more than three hours), the expander torque is increased step by step. Flow rates are almost not changed at low expander torques. Such flow rate is about 650 kg/h. However, when the expander torque exceeds 15.54 Nm, flow rates are decreased and oscillating. The phenomenon is more obvious at the expander torque of 29.61 Nm. The oscillating amplitude attains about ±50 kg/h at extremely high expander torque. Fig. 4 demonstrates the match between flow rates and expander torques.

3.2. The operation at the oil temperature of 140 °C

This section describes the ORC operation at $T_{oil,i} = 140$ °C. The match between pump and expander is focused. The effect of heat source temperature will be described in the next section.

The pumping behavior: Fig. 5a shows flow rates at various frequencies and expander torques. The curves are classified as three groups in terms of $f = 7$, 8 and 12 Hz. For each group of f, the dashed line represents the ideal flow rate, and the dynamic curve indicates

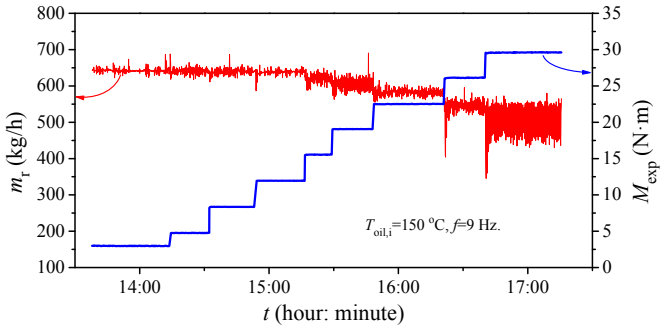

Fig. 4. Dynamic flow rates by the step increase of the expander torque during ORC operation.

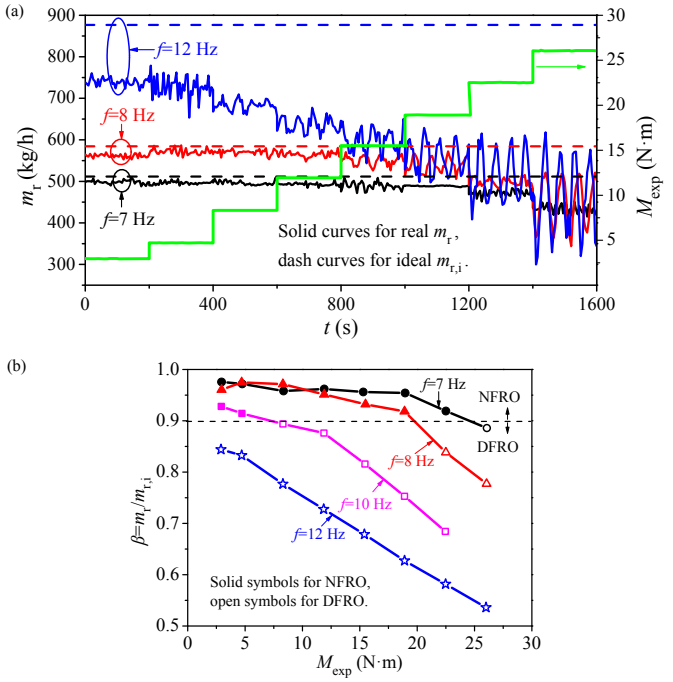

Fig. 5. Dynamic flow rates by step increases of expander torques at various pump frequencies (a) and flow rate ratios dependent on pump frequencies and expander torques (b).

the measured values. At $f = 7$ Hz, mass flow rates are quite stable and approach the ideal value, except when the expander torque is significant large (black curves). Beyond $M_{exp} = 22.53$ Nm, mass flow rates are decreased and oscillating. When the pump frequency is

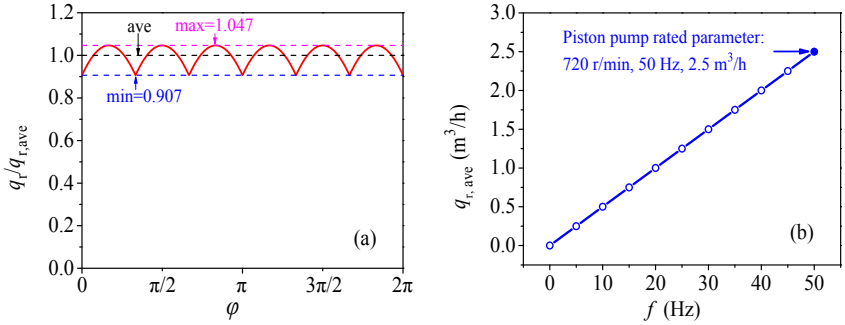

Fig. 3. Piston pump flow rates in one cycle (a) and ideal average flow rate versus pump frequencies (b).

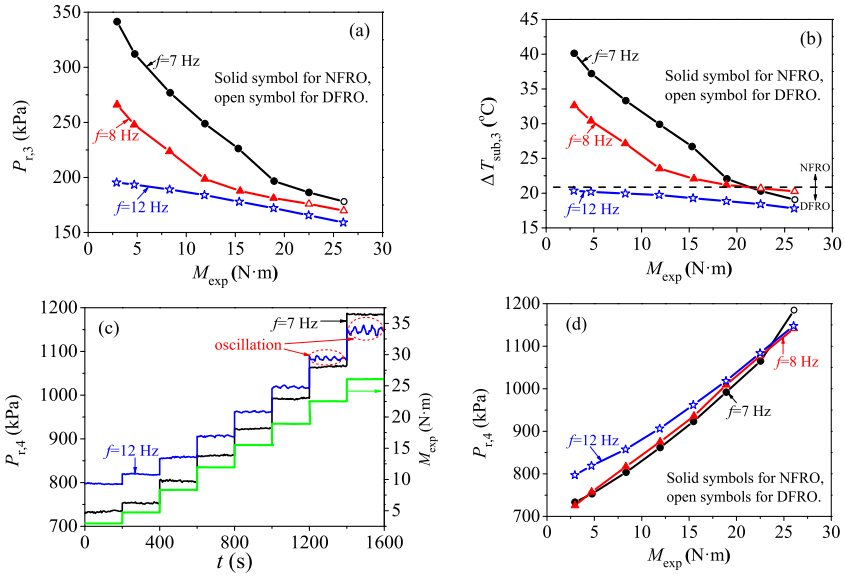

Fig. 6. Pressures and liquid subcoolings at the pump inlet (a and b), pressures at the pump outlet (c and d).

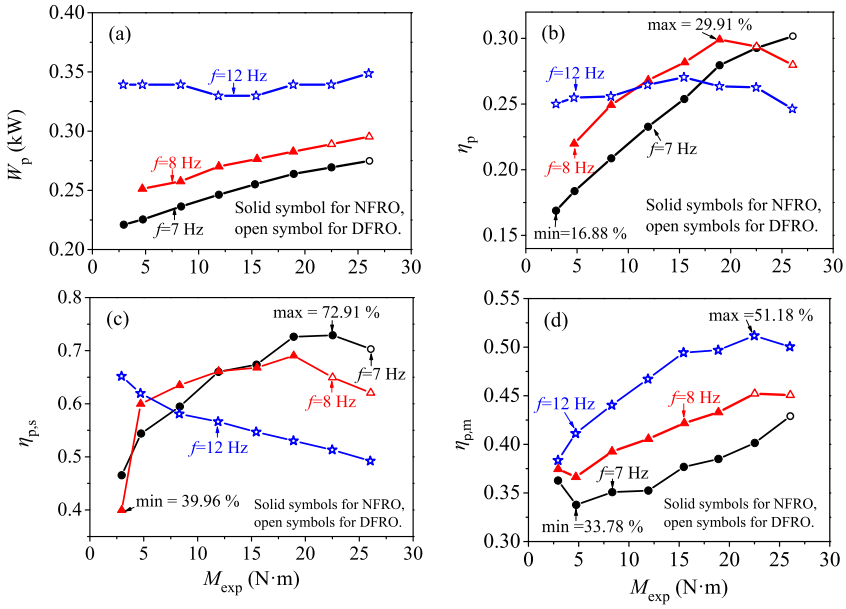

Fig. 7. Pumping powers (a), measured pump efficiencies (b), calculated pump isentropic efficiencies (c) and pump mechanical efficiencies (d).

increased, the transition from stable to unstable flow rates is shifted to lower expander torques. For example, flow rates at $f = 8$ Hz begins to decrease and oscillate at $M_{exp} = 15.51$ Nm (red curves (in the web version)). The blue curves (in the web version) at $f = 12$ Hz show significant deviation of measured flow rates from ideal value, even at low torques. The flow rate decrease and oscillation are apparent at $M_{exp} = 2.96$ Nm, indicating the poor match of pump frequency and expander torque.

The flow rate coefficient is defined as $\beta = m_r/m_{r,i}$, where $m_{r,i}$ is the ideal flow rate. Solid symbols having $\beta > 0.9$ represent NFRO (Normal Flow Rate Operation), and open symbols with $\beta < 0.9$ indicate DFRO (Deviated Flow Rate Operation). Fig. 5b summarizes results at $f = 7$, 8, 10 and 12 Hz. Most of data points at $f = 7$ and 8 Hz are in the NFRO regime except one data point for $M_{exp} > 18.91$ Nm. The pump frequencies of 10 and 12 Hz behave sharp decrease of β and most of data points are in the DFRO regime. Thus, the high pump frequency is not suitable for the present ORC.

Fig. 6 plots pump inlet pressure ($P_{r,3}$), outlet pressure ($P_{r,4}$) and pump inlet liquid subcooling ($\Delta T_{sub,3}$). The pump inlet pressures are decreased and outlet pressures are increased with increases in expander torques (see Fig. 6a and d). An exception is found for $f = 12$ Hz, in which pump inlet pressures are not sensitive to expander torques (see blue (in the web version) curve in Fig. 6a). The pump inlet liquid subcooling is important for the pump operation. The nearly saturation liquid at pump inlet causes cavitation to decrease and oscillate flow rates (see Fig. 6c), which should be avoided. Fig. 6b shows decreased liquid subcooling versus expander torques. The solid symbols represent NFRO, which can be satisfied if $\Delta T_{sub,3} > 20.7$ °C. All data points at $f = 12$ Hz belong to DFRO, caused by $\Delta T_{sub,3} < 20.7$ °C.

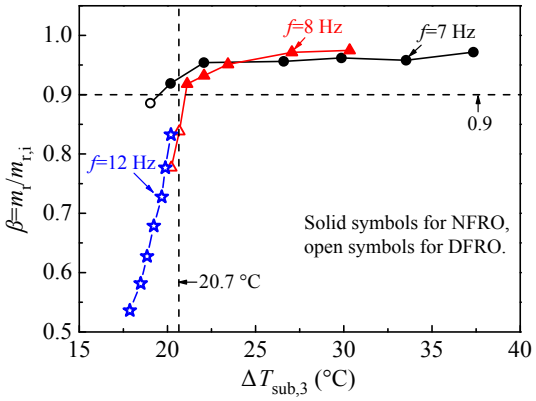

Fig. 8. Flow rate coefficients versus liquid subcoolings at the pump inlet.

Fig. 7a–b shows measured pump powers (W_p) and efficiencies (η_p) dependent on pump frequencies and expander torques, showing increased W_p and η_p with increases of f and M_{exp}. The effect of expander torques on W_p and η_p becomes weak at $f = 12$ Hz. The maximum pump efficiency is 29.91%, occurring at $f = 8$ Hz and $M_{exp} = 18.91$ Nm. The η_p values do not change versus M_{exp} and are about 26% at $f = 12$ Hz.

The pump isentropic efficiency ($\eta_{p,s}$) is important to characterize pump performance (see Fig. 7c). The solid and open symbols represent NFRO and DFRO, respectively. It is found that $\eta_{p,s}$ is increased with increases in M_{exp} for NFRO, indicating the improved pump performance. Once DFRO occurs, $\eta_{p,s}$ is decreased, showing the deteriorated performance. For normal operation, $\eta_{p,s}$ can be 60–72%.

The pump mechanical efficiency characterizes the pump mechanical performance. Fig. 7d shows the increased mechanical efficiencies with increases in pump frequencies and expander torques. The increase of expander torque increases the system pressure, while the increase of pump frequency raises the flow rate. The maximum mechanical efficiency is 51%.

Pump is an important component, which is still in developing stage for ORC. This paper explores the effect of pump performance on ORC. The piston pump having a wide range of flow rates is selected. Besides, the practical flow rate is difficult to approach the rated value. Thus, an oversized pump with higher rated flow rate is used in this study. Due to similar reason, other studies such as Refs. [13,33] also used the oversized pumps. Zhou et al. [13] used the practical flow rates which are 30% of the rated value. Alternatively, Wang et al. [33] used the practical flow rates which are 10–44% of the rated value.

The equilibrium thermodynamic analysis assumes nearly saturated liquid at pump inlet, which is not suitable for ORC operation. A specific liquid subcooling is necessary, due to the non-equilibrium energy conversion in the pump. Fig. 8 shows flow rate coefficients smaller than 0.9 for liquid subcooling less than 20.7 °C. Flow rates are oscillating and cavitation occurs in the pump. Noise and vibration are detected at such states. However, flow rate coefficients can be up to 0.95 without cavitation, when liquid subcooling is beyond 20.7 °C.

Cavitation widely happens in pumps and rotating machines. The phenomenon is caused by dynamic variations of pressures and temperatures in the pump. During the liquid suction stage, liquid pressure is instantaneously decreased to approach the saturation pressure corresponding to the liquid temperature. Miniature bubbles appear during the pressure decrease stage. During the liquid discharge stage, the pressure is sharply increased. Miniature bubbles are collapsed and disappear. In a full pumping cycle, the bubble formation and collapse cause shock wave. The shock wave is harmful and shortens the pump lifetime. It also causes unstable flow rates.

Cavitation is more serious for organic fluid pumps. This is because most organic liquids have significantly lower evaporation temperature and smaller latent heat of evaporation compared with water. In other words, miniature bubbles are more easily to be formed in organic fluid pumps.

There are fewer investigations regarding cavitation in organic fluid pumps. Lakew and Bolland [24] used the zeotropic mixture of R245fa/R365mfc as the working fluid. The liquid subcooling at pump inlet was 13 °C. Quoilin et al. [52] used the diaphragm pump in the ORC loop. They suggested the liquid subcooling at pump inlet in the range of 20–44 °C. Reid [53] reported experimental studies on ORC. A centrifugal pump was used. The maximum pump efficiency was only 7%. The liquid subcooling was not reported in his paper.

The measure to avoid cavitation is to increase liquid subcooling at pump inlet, such as reported in the present paper. An alternative way is to increase static hydraulic pressure head at pump inlet, corresponding to rise of the liquid subcooling.

The left issue is the pump efficiency. The isentropic efficiency, mechanical efficiency and overall efficiency are recorded as $\eta_{p,s}$, $\eta_{p,m}$ and η_p respectively. They have the following relationship: $\eta_p = \eta_{p,s}\eta_{p,m}$. The maximum isentropic efficiency is up to 72.9%, which is not low compared with other studies. The assumed isentropic efficiency covers the range of 65–85% in Ref. [50]. However, the mechanical efficiency is not considered in the literature. The present study obtains $\eta_{p,m}$ in the range of 35–51% (see Fig. 7d). Physically, the mechanical efficiency represents how much of the electricity can be converted to the useful power for fluid enthalpy increment. Various destructions exist such as heat transferred from pump to environment, friction loss between static part and moving part of the pump. The mechanical efficiency is relatively low for small scale ORC. It can be increased if one increases the ORC capacity. The relatively low mechanical efficiency yields lower overall pump efficiencies of 17–30% (see Fig. 7b).

Very few studies reported overall pump efficiencies. Quoilin et al. [52] reported the measured pump efficiency of 15%. Reid [53] measured the pump efficiency of 7%. Our measured pump efficiencies are apparently larger than those reported in Refs. [52,53].

The expander behavior: When expander torques are increased, pressures ($P_{r,1}$) are increased, but vapor temperatures ($T_{r,1}$) and superheatings ($\Delta T_{sup,1}$) are decreased, at the expander inlet (see Fig. 9). At $f = 12$ Hz, $\Delta T_{sup,1}$ is quite small corresponding to near saturation vapor at the expander inlet (see Fig. 9c). The vapor superheating at the expander inlet is an important parameter to influence ORC performance. Fig. 10 plots measured expander powers versus vapor superheating degrees. Expander powers show parabola shape versus vapor superheating degrees. The maximum expander power appears at $\Delta T_{sup,1} = 17$ °C at $f = 7$ Hz, and $\Delta T_{sup,1} = 13$ °C at $f = 8$ Hz. The measurements significantly deviate from equilibrium thermodynamic analysis, which notes the maximum power occurring at the inlet saturation vapor.

Non-equilibrium evaporation heat transfer in the evaporator explains the reason [54]. During the convective evaporation heat transfer in the tube, liquid films exist on tube wall. Shear-stress on the liquid–vapor interface entrains liquid droplets in the vapor. The vapor has the saturation temperature but liquid droplets have lower temperature than the vapor. The temperature difference between vapor and liquid droplets is called the thermal non-equilibrium effect. When liquid droplets enter the expander, they attack the expander blade. The shock wave is created in a very short period of time (10^{-8} s scale [55]) during the droplet attacking process. A strong mechanical force is formed for such attacking. The

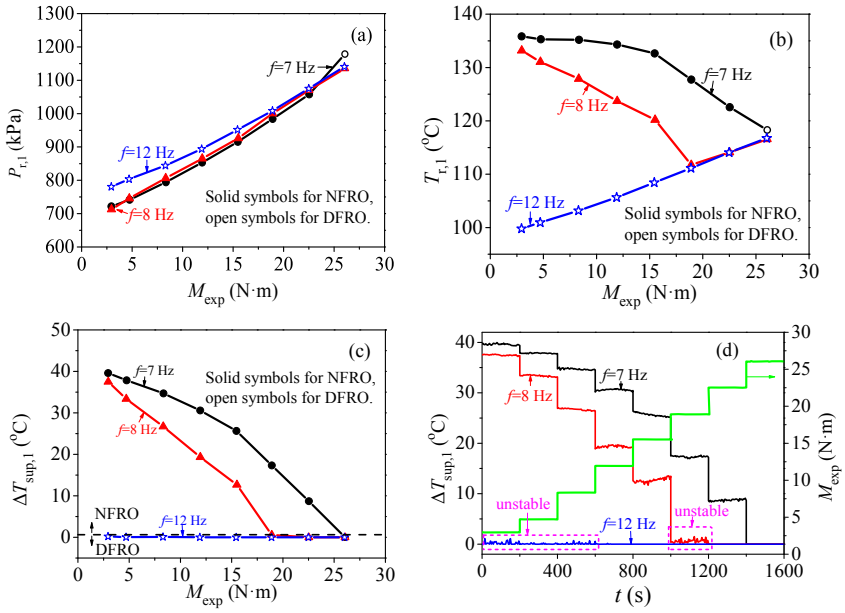

Fig. 9. Expander inlet pressures (a), temperatures (b) and vapor superheating degrees (c and d).

droplet induced shock wave and mechanical force disturb the normal flow field in the expander. Thus, the expander power cannot reach the maximum value. Such phenomenon also shortens the expander lifetime.

Fewer studies investigated vapor superheatings. Gao et al. [35] used the scroll expander with R245fa as the working fluid. They found the maximum expander power at the vapor superheating of 28 °C. Lee et al. [45] used the screw expander and plate heat exchangers. The system was unstable and thermal efficiency was low for vapor superheatings lower than 10 °C.

The useful way to avoid the droplet attacking process is to increase the vapor superheating degrees, under which apparent heat transfer takes place between superheated vapor and liquid droplets. Thus, liquid droplets can be completely evaporated to achieve a pure vapor at the expander inlet, explaining why a vapor superheating of 13 °C is necessary to have the maximum expander power. An alternative way to avoid liquid droplet is to set a two-phase separator, in which liquid droplets can be removed.

Fig. 11 shows decreased pressures, temperatures and vapor superheating degrees at expander outlet. The effect of expander torques on the parameters at the expander outlet becomes weak at $f = 12$ Hz. The expansion ratio ε is defined as expander inlet pressure divided by outlet pressure, i.e. $\varepsilon = P_{r,1}/P_{r,2}$. The increase of M_{exp} increases expansion ratios (see Fig. 12a), but decreases expander rotating speeds (see Fig. 12b). The measured expander powers (W_{exp}) have parabola distribution versus expander torques (see Fig. 12c). Larger expander powers happen with M_{exp} in the range of 12–19 Nm.

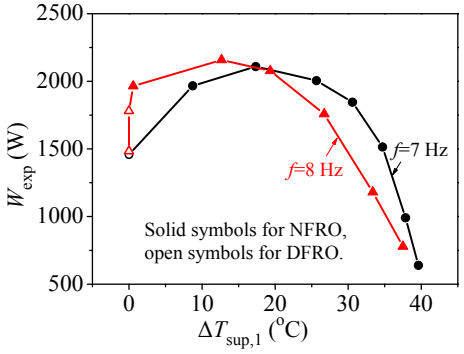

Fig. 10. Measured expander powers versus vapor superheating degrees at the expander inlet.

Fig. 12d shows measured expander power (W_{exp}) divided by enthalpy difference decided value ($W_{exp,cal}$), showing parabola shape versus M_{exp}. The better cases have $W_{exp}/W_{exp,cal}$ of 0.8–0.9. Fig. 12e shows expander efficiencies versus expander torques. The measured expander efficiencies (η_{exp}) are apparently smaller than the isentropic efficiencies ($\eta_{exp,s}$). The isentropic efficiencies ($\eta_{exp,s}$) reach 0.60–0.88. It cannot reflect real expander working state. The enthalpy difference across expander may not completely convert to useful power. Part of the enthalpy difference is consumed by energy dissipation. The measured expander efficiencies are 40–60%.

One may be interested in pumping power divided by expander power (W_p/W_{exp}, see Fig. 12f). The measured W_p/W_{exp}, and enthalpy decided $W_{p,cal}/W_{exp,cal}$ are shown. The measured W_p/W_{exp} covers the range of 13–30%. The calculated $W_{p,cal}/W_{exp,cal}$ covers the range of 3.5–7.5%.

The system behavior: Attention is paid to net power (W_{net}), which is defined as expander power subtracting pumping power (see Eq. (2)). Net thermal efficiency is defined as net power divided by heat received from the heat source (see Eq. (3)). We saw the parabola distribution of net powers versus expander torques (see Fig. 13a). The maximum net power reaches 1881.3 W at $M_{exp} = 15.51$ Nm.

Fig. 13b shows thermal efficiencies versus expander torques. The solid and dashed curves represent measured (see Eq. (3)) and calculated efficiencies (see Eq. (12)). The calculated thermal efficiencies are increased with increases in M_{exp}, with the maximum value of 8.25%. The measured thermal efficiencies show the parabola shape versus M_{exp}, with the maximum value of 5.78% at $M_{exp} = 15.51$ Nm.

Three points of *a*, *b* and *c* are marked in Fig. 13a, having the vapor superheating degrees of 33.4 °C, 12.7 °C and 0 °C, respectively. The *T-s* curves are shown in Fig. 14. Fig. 10 told us that the expander power attains maximum at the vapor superheating degree of 13 °C

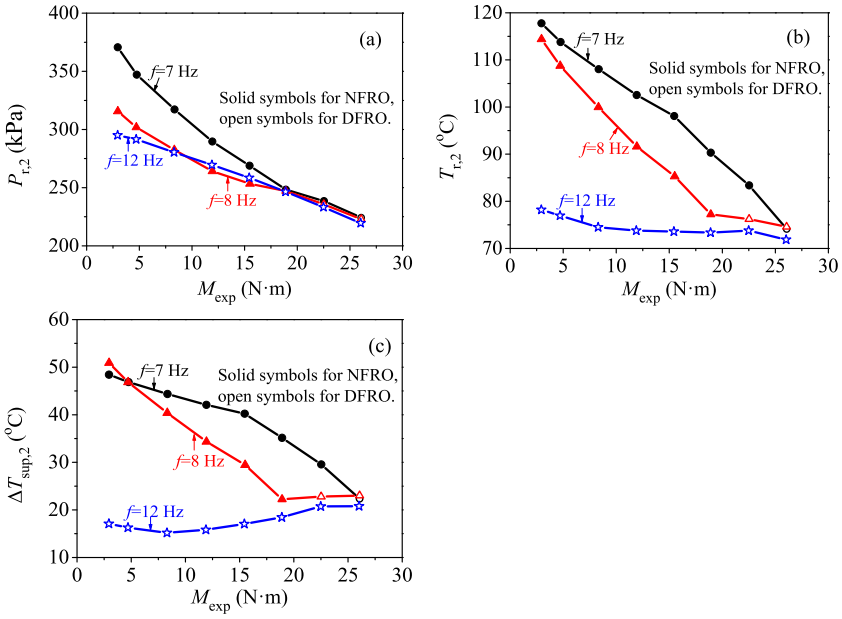

Fig. 11. Expander outlet pressures (a), temperatures (b) and vapor superheatings (c).

(point *b*). Deviation from the vapor superheating degree of 13 °C decreases expander powers, which is the main reason to cause the parabola distribution of W_{net} versus M_{exp} (see Fig. 13a). The net power is also influenced by the heat received from the heat source, which is 38.4 kW, 35.2 kW and 28.1 kW at point *a*, *b* and *c*. The lower net power at point *c* is partially due to the lower heat received from the heat source.

Due to decreased vapor superheating degrees, calculated thermal efficiencies are increased from point *a* to *c* (see dashed curves in Fig. 13b), which is consistent with the equilibrium

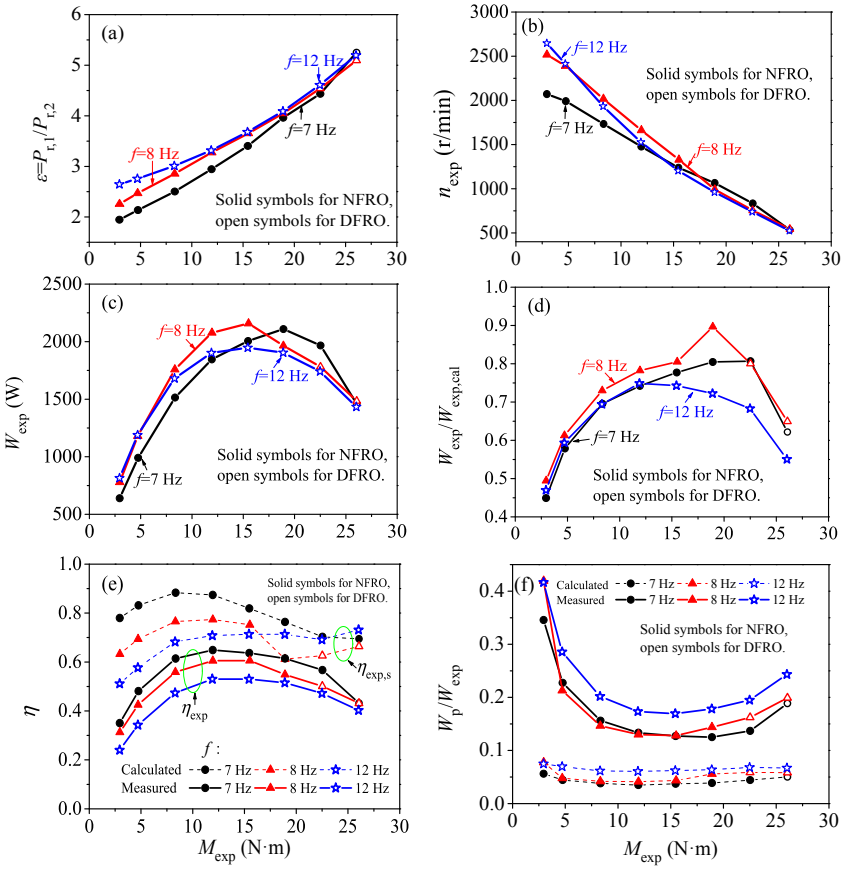

Fig. 12. Expansion ratios (a), rotating speeds (b), measured expander powers (c), $W_{exp}/W_{exp,cal}$ (d), expander efficiency (e) and W_p/W_{exp} (f).

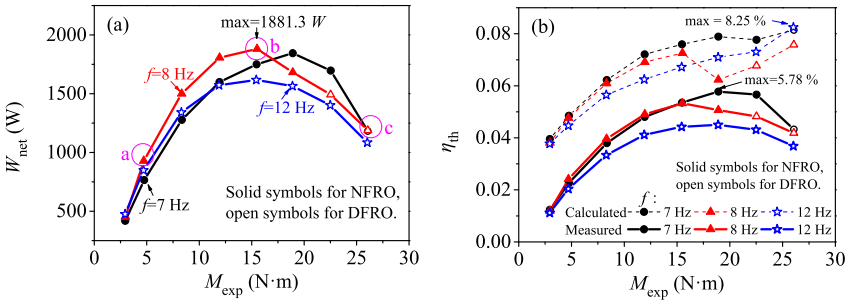

Fig. 13. System net powers (a) and thermal efficiencies (b).

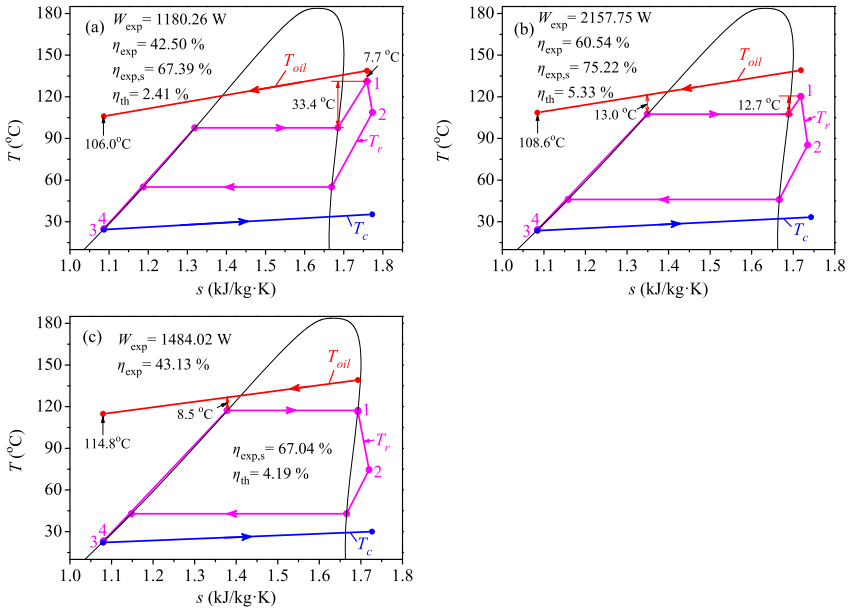

Fig. 14. Three *T*–*s* curves at the three points of a, b and c.

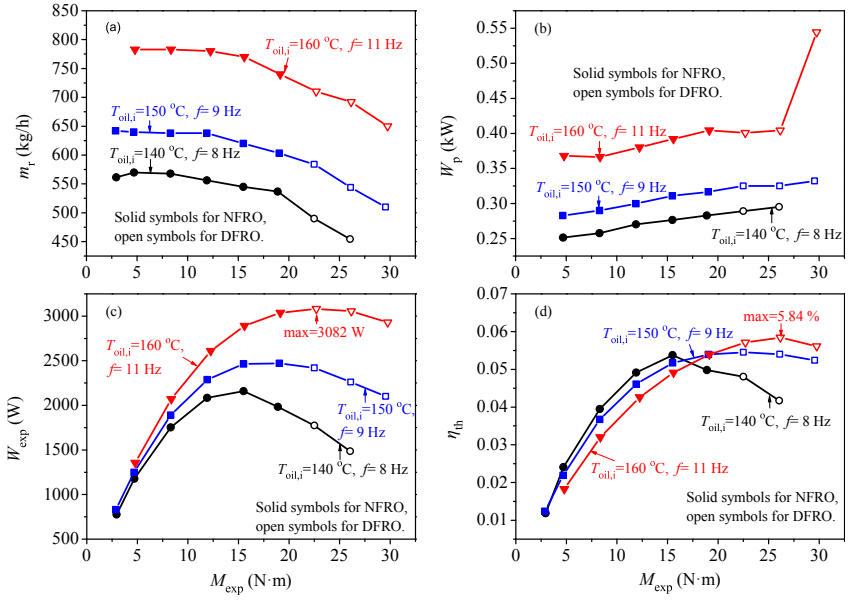

Fig. 15. Effect of heat source temperatures on system performance (maximum power of 3082 W appeared at $T_{oil,i}$ = 160 °C).

thermodynamic analysis. Measured thermal efficiencies attain maximum at point *b* for which the vapor superheating degree is 13 °C (see solid curves in Fig. 13b). This does not support the equilibrium thermodynamic analysis. The saturation vapor at the expander inlet causes disturbed flow field due to liquid droplet induced shock wave in the expander. The varied expander efficiency (η_{exp}) is caused by the varied pressure and temperature distribution in the expander. The highest expander efficiency is 60.54% at the vapor superheating degree of 13 °C (see Fig. 14b). However, η_{exp} is decreased to 43.13% at point *c* (saturation vapor inlet, see Fig. 14c). In summary, saturation vapor at expander inlet worsens the expander and system performance.

3.3. The effect of heat source temperatures

Fig. 15 summarizes results for the oil inlet temperatures of 140, 150 and 160 °C. The R123 flow rates, pumping powers, expander powers and thermal efficiencies are the measured ones. The parameters dependent on pump frequencies and expander torques are similar for all the three oil temperatures. Mass flow rates, pumping powers and expander powers achieve significant increase with increase of heat source temperatures. Fig. 15c shows expander powers versus expander torques. The maximum expander power is 2160 W at $T_{oil,i}$ = 140 °C, but it is 3082 W at f = 11 Hz, M_{exp} = 22.70 Nm and $T_{oil,i}$ = 160 °C. Thermal efficiencies are intercrossed with the three heat source temperatures. They are higher for low heat source temperatures and low expander torques (M_{exp} < 15.51 Nm), but they are higher for high heat source temperatures and large expander torques (see Fig. 15d). The increased heat source temperatures should have larger expander torques to have better performance. The increased heat source temperatures also need higher pump frequencies. The higher pump frequency of f = 11 Hz is not suitable for the heat source temperature of 140 °C, but it is suitable for the 160 °C oil temperature. The optimal pump frequencies and expander torques are f < 10 Hz and M_{exp} = 11.95–18.91 Nm at $T_{oil,i}$ = 140 °C. When $T_{oil,i}$ equals to 160 °C, the optimal pump frequency is f = 11 Hz and expander torques are M_{exp} = 19.15–26.15 Nm, respectively.

Fig. 16 shows effect of heat source temperatures on measured expander efficiencies. The curves display parabola shapes, which are similar to each other for three heat source temperatures. The maximum expander efficiency attains 60.6%, which is almost highest compared with measured values in the literature (see Table 1). Low expander torques yield ultra high vapor superheating degrees at expander inlet to have small expander efficiencies. Expander efficiencies are increased with increases in expander torques (or decreases in vapor superheatings at expander inlet), until maximum is reached, beyond which the vapor superheating becomes small to reach the saturation vapor. The liquid droplets entrained in vapor not only decrease expander efficiencies, but also shorten expander lifetime, explaining the parabola distribution of expander efficiencies versus expander torques.

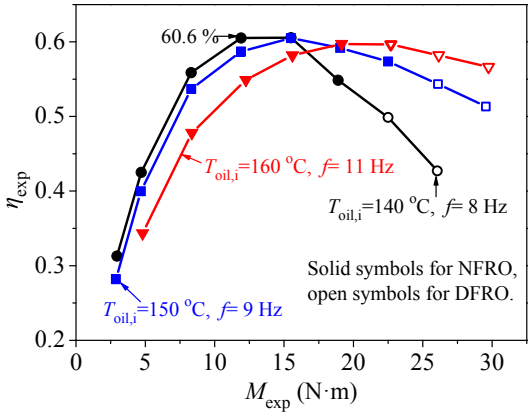

Fig. 16. Expander efficiency versus expander torques for different heat source temperatures.

3.4. Comparison with other studies

Many equilibrium thermodynamic analyses have been reported in the literature [6,7,16,26]. The analysis does not consider the vapor–liquid flow and heat transfer in various components. The assumptions are the near saturation liquid at pump inlet and saturation vapor at expander inlet. Other assumptions include isentropic efficiencies of pump in the range of 65–85% [50] and of the expander in the range of 75–87% [25,31,32]. The present measurements note that saturation liquid at pump inlet and saturation vapor at expander inlet may not be suitable for practical ORC design and operation. The ORC development behaves multidisciplinary principle.

The present paper investigates the match between pump and expander. The adjusting parameters are pump frequencies (f) and expander torques (M_{exp}). The pump frequencies of 7 and 8 Hz adapt the whole range of expander torques. High pump frequencies (f > 10 Hz) adapt low expander torques only.

Pump frequencies and expander torques affect flow rates, pressures and temperatures. Low pump frequencies of 7 and 8 Hz yield stable flow without cavitation. Flow rates are decreased and oscillating at high pump frequencies (f > 10 Hz), under which pump cavitation appears. Ultra-low expander torques generate sufficiently high vapor superheatings to decrease expander efficiencies, consistent with the equilibrium thermodynamic analysis. Ultra-high expander torques achieve saturation vapor at expander inlet, involving liquid droplets induced shock wave to decrease expander powers and efficiencies, which cannot be treated by the equilibrium thermodynamics. For the 140 °C oil temperature, the optimal expander torque is about 15 Nm. The range of 10–25 Nm is acceptable.

Fig. 8 shows flow rate coefficients versus liquid subcoolings. A liquid subcooling of 20 °C is necessary to avoid the shock wave caused cavitation in the pump. The expander powers show parabola shape versus vapor superheatings at expander inlet. The optimal vapor superheating is about 13 °C, beyond which decreases the expander power (see Fig. 10). The measured expander efficiencies also display the parabola distribution versus expander toques (see Fig. 16). The mechanisms and measures to avoid cavitation in pumps and expanders are discussed.

There are fewer experimental studies on the match between pump and expander (see Table 1). The heat source temperatures are in the range of 41–485 °C [13,18,35–47]. The organic fluids are R123, R245fa and others [13,35–39]. Most ORCs have ~1 kW capacity [37–43]. Very few studies report ~10 kW power output or larger [45–47]. The isentropic efficiencies of pumps are less reported. The overall pump efficiencies are 7–25% [49,52,53]. This study measured overall pump efficiencies of 16.88–29.91%, slightly larger than 7–25% in Refs. [49,52,53].

The isentropic efficiencies of the expander are reported in the range of 4.55–85% in Refs. [39–43,56]. The measured expander efficiencies are not reported. The measured expander efficiencies are 24.03–64.88% in this study.

The ORC performances versus liquid subcoolings at pump inlet and vapor superheatings at expander inlet are thoroughly investigated in this paper. Such relationship is not seen in the literature. Lakew and Bolland [24] used the liquid subcooling at pump inlet of 13 °C. Quoilin et al. [52] suggested the liquid subcooling at pump

inlet of 20–44 °C. Gao et al. [35] used the scroll expander and found the maximum expander power at the vapor superheating of 28 °C. Lee et al. [45] used the screw expander and found the unstable system and low system thermal efficiency when the vapor superheating was smaller than 10 °C.

In summary, the equilibrium thermodynamics overestimate the ORC performance. A set of assumptions should be relied on the measured values for practical ORC design and operation. The flow, heat transfer and energy conversion should be investigated in heat exchangers, pumps and expanders. The cavitation in pumps and expanders for organic fluids should be paid great attention. The available studies on cavitation are for water-vapor system. The problem becomes serious for organic liquid–vapor systems.

4. Conclusions

The new findings are summarized as follows:

- The match between pump and expander is investigated. Pump frequencies and expander torques are adjusting parameters. Lower pump frequencies ($f < 10$ Hz) adapt the whole range of expander torques. Higher pump frequencies ($f > 10$ Hz) adapt low expander torques only.
- Lower pump frequencies ($f < 10$ Hz) yield stable flow. Higher pump frequencies cause unstable flow with cavitation.
- Ultra-low expander torques generate sufficiently high vapor superheatings to decrease expander efficiencies. Ultra-high expander torques achieve saturation vapor at expander inlet, involving liquid droplets induced shock wave to worsen expander performance. An optimal range of expander torques exists to have better expander performance.
- A liquid subcooling of 20 °C is necessary to avoid pump cavitation. Expander powers and efficiencies show parabola shapes versus expander torques, or vapor superheatings at expander inlet. The optimal vapor superheating is 13 °C.
- The increase of heat source temperatures enlarges suitable ranges of pump frequencies and expander torques.
- For pumps and expanders, the cavitation mechanisms are analyzed and measures to avoid cavitation are discussed.
- This paper notes the overestimation of ORC efficiencies by equilibrium thermodynamic analysis. Assumptions should be dependent on experiments. Future studies are suggested on organic fluid flow, heat transfer and energy conversion in various components.

Acknowledgments

This work was financially supported by the Natural Science Foundation of China (51210011 and 51436004).

References

[1] Chan CW, Ling-Chin J, Roskilly AP. A review of chemical heat pumps, thermodynamic cycles and thermal energy storage technologies for low grade heat utilisation. Appl Therm Eng 2013;50:1257–73.
[2] Tchanche BF, Lambrinos G, Frangoudakis A, Papadakis G. Low-grade heat conversion into power using organic Rankine cycles – a review of various applications. Renew Sustain Energy Rev 2011;15:3963–79.
[3] Velez F, Segovia JJ, Martin MC, Antonlin G, Chejne F, Quijano A. A technical, economical and market review of organic Rankine cycles for the conversion of low-grade heat for power generation. Renew Sustain Energy Rev 2012;16:4175–89.
[4] Cheng WL, Li TT, Nian YL, Wang CL. Studies on geothermal power generation using abandoned oil wells. Energy 2013;59:248–54.
[5] Hettiarachchia HDM, Golubovica M, Worek WM, Ikegami Y. Optimum design criteria for an organic Rankine cycle using low-temperature geothermal heat sources. Energy 2007;32:1698–706.
[6] Guo T, Wang HX, Zhang SJ. Fluids and parameters optimization for a novel cogeneration system driven by low-temperature geothermal sources. Energy 2011;36:2639–49.
[7] Liu Q, Duan YY, Yang Z. Performance analyses of geothermal organic Rankine cycles with selected hydrocarbon working fluids. Energy 2013;63:123–32.
[8] Ali MT, Fath HES, Armstrong PR. A comprehensive techno-economical review of indirect solar desalination. Renew Sustain Energy Rev 2011;15:4187–99.
[9] Li CN, Goswami Y, Stefanakos E. Solar assisted sea water desalination: a review. Renew Sustain Energy Rev 2013;19:136–63.
[10] Yari M, Mehr AS, Mahmoudi SMS. Thermodynamic analysis and optimization of a novel dual-evaporator system powered by electrical and solar energy sources. Energy 2013;61:646–56.
[11] Xia GH, Sun QX, Cao X, Wang JF, Yu YZ, Wang LS. Thermodynamic analysis and optimization of a solar-powered transcritical CO_2 (carbon dioxide) power cycle for reverse osmosis desalination based on the recovery of cryogenic energy of LNG (liquefied natural gas). Energy 2014;66:643–53.
[12] Quoilin S, Aumann R, Grill A, Schuster A, Lemort V, Spliethoff H. Dynamic modeling and optimal control strategy of waste heat recovery organic Rankine cycles. Appl Energy 2011;88:2183–90.
[13] Zhou NJ, Wang XY, Chen Z, Wang ZQ. Experimental study on organic Rankine cycle for waste heat recovery from low-temperature flue gas. Energy 2013;55:216–25.
[14] Wang CJ, He BS, Yan LB, Pei XH, Chen SN. Thermodynamic analysis of a low-pressure economizer based waste heat recovery system for a coal-fired power plant. Energy 2014;65:80–90.
[15] Wang DX, Ling X, Peng H, Liu L, Tao LL. Efficiency and optimal performance evaluation of organic Rankine cycle for low grade waste heat power generation. Energy 2013;50:343–52.
[16] Xu JL, Liu C. Effect of the critical temperature of organic fluids on supercritical pressure organic Rankine cycles. Energy 2013;63:109–22.
[17] Chen QC, Xu JL, Chen HX. A new design method for organic Rankine cycles with constraint of inlet and outlet heat carrier fluid temperatures coupling with the heat source. Appl Energy 2012;98:562–73.
[18] Zhang YQ, Wu YT, Xia GD, Ma CF, Ji WN, Liu SW, et al. Development and experimental study on organic Rankine cycle system with single-screw expander for waste heat recovery from exhaust of diesel engine. Energy 2014;77:499–508.
[19] Yang K, Zhang HG, Song SS, Yang FB, Liu H, Zhao GY, et al. Effects of degree of superheat on the running performance of an organic Rankine cycle (ORC) waste heat recovery system for diesel engines under various operating conditions. Energies 2014;7:2123–45.
[20] Maraver D, Sin A, Royo J, Sebastian F. Assessment of CCHP systems based on biomass combustion for small-scale applications through a review of the technology and analysis of energy efficiency parameters. Appl Energy 2013;102:1303–13.
[21] Ahmadi P, Dincer I, Rosen MA. Thermoeconomic multi-objective optimization of a novel biomass-based integrated energy system. Energy 2014;68:958–70.
[22] Tanczuk M, Ulbrich R. Implementation of a biomass-fired co-generation plant supplied with an ORC (organic Rankine cycle) as a heat source for small scale heat distribution system – a comparative analysis under Polish and German conditions. Energy 2013;62:132–41.
[23] Saleh B, Koglbauer G, Wendland M, Fischer J. Working fluids for low-temperature organic Rankine cycles. Energy 2007;32:1210–21.
[24] Lakew AA, Bolland O. Working fluids for low-temperature heat source. Appl Therm Eng 2010;30:1262–8.
[25] Xu JL, Yu C. Critical temperature criterion for selection of working fluids for subcritical pressure organic Rankine cycles. Energy 2014;74:719–33.
[26] He C, Liu C, Gao H, Xie H, Li YR, Wu SY, et al. The optimal evaporation temperature and working fluids for subcritical organic Rankine cycle. Energy 2012;38:136–43.
[27] Velez F, Chejne F, Antolin G, Quijano A. Theoretical analysis of a transcritical power cycle for power generation from waste energy at low temperature heat source. Energy Convers Manage 2012;60:188–95.
[28] Chys M, van den Broek M, Vanslambrouck B, De Paepe M. Potential of zeotropic mixtures as working fluids in organic Rankine cycles. Energy 2012;44:623–32.
[29] Roy JP, Mishra MK, Misra A. Performance analysis of an organic Rankine cycle with superheating under different heat source temperature conditions. Appl Energy 2011;88:2995–3004.
[30] Kim KH, Ko HJ. Exergetical performance assessment of organic Rankine cycle with superheating. Appl Mech Mater 2012;234:69–73.
[31] Chacartegui R, Muñoz de Escalona JM, Sánchez D, Monje B, Sánchez T. Alternative cycles based on carbon dioxide for central receiver solar power plants. Appl Therm Eng 2011;31:872–9.
[32] Yamamoto T, Furuhata T, Arai N, Mori Koichi. Design and testing of the organic Rankine cycle. Energy 2001;26:239–51.
[33] Wang XD, Zhao L, Wang JL, Zhang WZ, Zhao XZ, Wu W. Performance evaluation of a low-temperature solar Rankine cycle system utilizing R245fa. Sol Energy 2010;84:353–64.
[34] Wang JL, Zhao L, Wang XD. An experimental study on the recuperative low temperature solar Rankine cycle using R245fa. Appl Energy 2012;94:34–40.
[35] Gao P, Jiang L, Wang LW, Wang RZ, Song FP. Simulation and experiments on an ORC system with different scroll expanders based on energy and exergy analysis. Appl Therm Eng 2015;75:880–8.

[36] Gu W, Weng YW, Cao GY. Testing and thermodynamic analysis of low-grade heat power generation system using organic Rankine cycle. Challenges Power Eng Environ 2007;1–2:93–8.
[37] Manolakos D, Papadakis G, Kyritsis S, Bouzianas K. Experimental evaluation of an autonomous low-temperature solar Rankine cycle system for reverse osmosis desalination. Desalination 2007;203:366–74.
[38] Manolakos D, Kosmadakis G, Kyritsis S, Papadakis G. On site experimental evaluation of a low-temperature solar organic Rankine cycle system for RO desalination. Sol Energy 2009;83:646–56.
[39] Mathias JA, Johnston JR, Cao JM, Priedeman DK, Christensen RN. Experimental testing of gerotor and scroll expanders used in, and energetic and exergetic modeling of, an organic Rankine cycle. J Energy Res Technol Trans ASME 2009;131:21–4.
[40] Lemort V, Quoilin S, Cuevas C, Lebrun J. Testing and modeling a scroll expander integrated into an organic Rankine cycle. Appl Therm Eng 2009;29:3094–102.
[41] Li T, Zhu JL, Fu WC, Hu KY. Experimental comparison of R245fa and R245fa/R601a for organic Rankine cycle using scroll expander. Int J Energy Res 2014;39:202–14.
[42] Qiu G, Shao Y, Li J, Liu H, Riffat SB. Experimental investigation of a biomass-fired ORC-based micro-CHP for domestic applications. Fuel 2012;96:374–82.
[43] Bracco R, Clemente S, Micheli D, Reini M. Experimental tests and modelization of a domestic-scale ORC (organic Rankine cycle). Energy 2013;58:107–16.
[44] Lee YR, Kuo CR, Wang CC. Transient response of a 50 kW organic Rankine cycle system. Energy 2012;48:532–8.
[45] Lee YR, Kuo CR, Liu CH, Fu BR, Hsieh JC, Wang CC. Dynamic response of a 50 kW organic Rankine cycle system in association with evaporators. Energies 2014;7:2436–48.
[46] Minea V. Power generation with ORC machines using low-grade waste heat or renewable energy. Appl Therm Eng 2014;69:143–54.
[47] Kang SH. Design and experimental study of ORC (organic Rankine cycle) and radial turbine using R245fa working fluid. Energy 2012;41:514–24.
[48] Song P, Wei M, Shi L, Danish SN, Ma CC. A review of scroll expanders for organic Rankine cycle systems. Appl Therm Eng 2015;75:54–64.
[49] Quoilin S, Van den Broek M, Declaye S, Dewallef P, Lemort V. Techno-economic survey of organic Rankine cycle (ORC) systems. Renew Sustain Energy Rev 2013;22:168–86.
[50] Borsukiewicz-Gozdur A. Pumping work in the organic Rankine cycle. Appl Therm Eng 2013;51:781–6.
[51] Cayer E, Galanis N, Desilets M, Nesreddine H, Roy P. Analysis of a carbon dioxide transcritical power cycle using a low temperature source. Appl Energy 2009;86:1055–63.
[52] Quoilin A, Lemort V, Lebrun J. Experimental study and modeling of an organic Rankine cycle using scroll expander. Appl Energy 2010;87:1260–8.
[53] Reid AD. Low temperature power generation using HFE-7000 in a Rankine cycle. San Diego: San Diego State University; 2010. Master thesis.
[54] Baehr HD, Stephan K. Heat and mass transfer. 2nd ed. Springer: Burlin; 2006. p. 477–9.
[55] Li N, Zhou Q, Chen X, Xu T, Hui S, Zhang D. Liquid drop impact on solid surface with application to water drope rosion on turbine blades, part I: nonlinear wave model and solution of one-dimensional impact. Int J Mech Sci 2008;50:1526–42.
[56] Yamada N, Tominaga Y, Yoshida T. Demonstration of 10-Wp micro organic Rankine cycle generator for low-grade heat recovery. Energy 2014;78:806–13.
[57] Miao Z, Xu JL, Yang XF, Zhou JH. Operation and performance of a low temperature organic Rankine cycle. Appl Therm Eng 2015;75:1065–75.
[58] Yun E, Kim D, Yoon SY, Kim KC. Experimental investigation of an organic Rankine cycle with multiple expanders used in parallel. Appl Energy 2015;145:246–54.
[59] Jung H-C, Taylor L, Krumdieck S. An experimental and modelling study of a 1 kW organic Rankine cycle unit with mixture working fluid. Energy 2015;81:601–14.
[60] Xia GD, Zhang YQ, Wu Y, Ma CF, Ji WN, Liu SW, et al. Experimental study on the performance of single-screw expander with different inlet vapor dryness. Appl Therm Eng 2015. http://dx.doi.org/10.1016/j.applthermaleng.2015.05.006.
[61] Peris B, Navarro-Esbrí J, Molés F, Martí JP, Mota-Babiloni A. Experimental characterization of an organic Rankine cycle (ORC) for micro-scale CHP applications. Appl Therm Eng 2015;79:1–8.

Nomenclature

C_P: heat capacity at constant pressure, kJ/(kg K)
f: piston pump's frequency, Hz
h: enthalpy, kJ/kg
m: mass flow rate, kg/h
M: torque, Nm
n: rotational speed, r/min
q: volume flow rate, m^3/h
Q: heat transfer rate, kW
P: pressure, kPa
s: entropy, kJ/(kg K)
T: temperature, °C
W: work (power), W
t: time, s
ΔT: temperature difference, °C
DFRO: deviated flow rate operation
NFRO: normal flow rate operation
MFM: mass flow mater

Greek symbols

β: coefficient of mass flow rate
ε: expander inlet and outlet pressure ratio
φ: rotational angle of the pump
η_{exp}: expander efficiency
η_p: pump efficiency
η_{th}: thermal efficiency

Subscripts

ave: average
c: cooling water
cr: critical
cal: calculated
con: condensing
ele: electrical
eva: evaporating
exp: expander
i: inlet or ideal
lubr: lubricant oil
N: rated parameter
m: mechanical
net: net output work
o: outlet
oil: heat conducting oil
p: pinch point
P: pump
r: working fluid (refrigerant)
s: isentropic
sat: saturated
sup: superheat
sub: subcooling
1–4: states in system
1: expander inlet state
2: expander outlet state
2′: condenser inlet state
3: pump inlet state /condenser outlet state
4: pump outlet state